Experimental investigation of magnetic-field-induced aggregation kinetics in nonaqueous ferrofluids

Junaid M. Laskar, John Philip,* and Baldev Raj
SMARTS, Metallurgy and Materials Group, Indira Gandhi Centre for Atomic Research, Kalpakkam 603 102, Tamilnadu, India
(Received 22 March 2010; revised manuscript received 22 June 2010; published 18 August 2010)

We investigate the influence of field ramp rate on the kinetics of magnetic dipole-dipole induced chainlike structure formation in a nonaqueous nanoparticle dispersion using light scattering studies. With increase in magnetic field, at a constant ramp rate, the transmitted light intensity diminishes and the transmitted light spot is transformed to a diffused ring due to scattering from the self-assembled linear aggregates. The decay rate of transmitted intensity increases up to an optimum ramp rate, above which the trend becomes reverse. At an optimum ramp rate, the minimum time for initial aggregation coincides with the exposure time where the intensity decay is fastest. The variation of transmitted intensity at different ramp rate is explained on the basis of initial aggregation time that depends on Brownian motion, dipolar magnetic attraction and multibody hydrodynamic interactions. The slope of the transmitted light intensity after the removal of magnetic field depends on the time required for dissociation of ordered linear structures. Disappearance of the ring pattern and the reappearance of original light spot, upon removal of the magnetic field, confirm the perfect reversibility of the linear aggregates. The observed concentration dependant decay rates are in good agreement with aggregation theory.

DOI: 10.1103/PhysRevE.82.021402 PACS number(s): 82.70.−y, 83.80.Gv, 64.70.Nd, 89.75.Fb

I. INTRODUCTION

Universality of colloidal aggregation dynamics in reaction and diffusion limited regimes is experimentally demonstrated almost two decades ago [1]. Since then, colloidal aggregation process has been a topic of interest for fundamental understanding and practical applications. Dynamic behavior of colloidal aggregation affects fundamental properties such as rheological behavior, phase separation, gel formation, and crystallization [2]. Among various dispersions, magnetic colloids offer the unique possibility of tuning the particle interaction by an external magnetic field that leads to interesting physical properties [3,4]. The tunability makes the magnetic colloidal system very appealing for fundamental understanding and also significantly increases their technological potential in biosensors, smart dampers, microfluids, optical grating, switches, filters etc. [5–10]. The dipolar colloidal system undergoes interesting structural changes under external field, e.g., linear chains or rods along field direction at low-particle loading and complex structures at high concentrations [11–22]. A strong foundation for field induced linear and lateral aggregation in superparamagnetic dispersions is laid by the Gast [13,15,23]. Liu *et al.* first demonstrated the field induced aggregation in ferrofluid emulsions and measured the column spacing, which follows a power law dependence on the column length [11]. Magnetic-field-induced ordering and microphase separation of aqueous ferrofluid is elegantly demonstrated using video microscopy [18]. With increasing magnetic field, they have shown transitions such as needlelike, columnar, glassy two-dimensional structure and sheet such as striped liquids in ferrofluid. The complex structural behavior in ferrofluid emulsion subjected to a slowly increasing magnetic field is beautifully demonstrated by Ivey *et al.* [21]. Field induced forces due to dipolar interaction among the particles in chains are examined theoretically [24]. The increase in length and upholding the chain structures under the influence of external field can be either reversible or irreversible depending upon the experimental conditions, enabling the magnetic colloids excellent model system to study the kinetics of cluster-cluster aggregation [25,26]. Different approaches are adopted to investigate aggregation dynamics of magnetic colloidal particles till now. Mostly, these include the determination of parameters like dynamic cluster size distribution, time-dependent structural evolution, aggregation rate and time. For irreversible aggregation process, usually the quantitative information about the temporal evolution is described by cluster size distribution $n_s(t)$, i.e., the number of clusters of size s per unit volume present in the system at time t. Several statistical variables can be calculated from $n_s(t)$, e.g., number of clusters present at time t, $N(t)$, or the mean cluster size $S(t)$ [27]. Computer simulations and experiments in different magnetic colloidal systems reveal a power-law behavior with time, given by [13,23,25,26,28–34]

$$S(t) \sim t^{z}, \quad N(t) \sim t^{-z'}, \tag{1}$$

where z and z' are the exponents. Most recent studies show that dynamic scaling exponents of aggregation in nondiffusion limited colloidal suspensions are not adequately described by diffusion limited cluster aggregation models, which expect the scaling exponents to be constant [35]. Their studies show that the dynamic scaling exponents for 10 μm particles increase with the particle concentration and the particle-particle free energy of interaction, where the scaling behavior is explained in terms of the long-ranged particle-particle interaction potential.

Using video-microscopy technique, the kinetic exponents at different field strength and concentration for several mag-

*Corresponding author; philip@igcar.gov.in

netic colloidal systems such as sulfonated polystyrene particles with iron oxide in water [26], superparamagnetic microparticles, made of magnetite grains randomly dispersed in a polymer matrix [13,23,29,30], paramagnetic nanoparticles [31,32] etc. are studied. Earlier, light scattering is used to measure the kinetic exponents in electrorheological fluids [33]. Similarly, other techniques such as scattering dichroism [34] and computer simulations [28] are also employed to obtain insight into kinetic exponents for different magnetic colloidal systems. Time-dependent structural evolution in magnetic colloidal system is also studied by molecular and stochastic dynamics simulation [36,37], Brownian dynamics [38], simulation based on a developed computer model [39], Raman spectroscopy [40], optical microscopy with digital image analysis [23,41], light scattering with electron microscopy [42], time resolved small angle neutron scattering [43]. Even though the aggregation times are estimated for various colloidal systems, they are not applicable in magnetic colloids as the aggregation mechanism is different [44]. Recently, we have shown that for very small particles i.e., $a \ll \lambda$, where α is the particle radius and λ is the wavelength of incident light; there is significant increase in the scattering due to increasing size of the aggregates under external field [45]. The, formation of field induced structures are studied by measuring the transmitted light and the scattered pattern. Also, such magnetic colloidal systems are excellent model system to study the scattering phenomena in different optical regimes because the scatterers' sizes can be tuned from Rayleigh regime ($a \ll \lambda$) at low field to Mie regime ($a \sim \lambda$) in the intermediate field range and finally to the geometrical regime ($a \gg \lambda$) at high-magnetic field. Though the measurement of transmitted and scattered light is established as a good technique to study the field aggregation process in dispersion of magnetic nanoparticles, the kinetics of the aggregation process is not studied earlier. Proper understanding of the parameters influencing aggregation kinetics in magnetic colloids is important from both fundamental and practical application point of view. Some of the interesting applications of field induced structures in ferrofluids and films are discussed [46,47]. Light scattering technique is used to probe the aggregation kinetics of magnetic colloidal systems. Aggregation times at different external fields are elegantly probed from the variation of forward scattered light and scattered pattern [48]. Also, aggregation rate at different external magnetic fields is found by measuring both the scattered light at small angle [49] and transmitted light [50]. Irrespective of some systematic studies of aggregation time in magnetic colloids, understanding of the underlying mechanism for aggregation time is still in an infancy [23].

In all the aggregation kinetics studies discussed above, both theoretical and experimental, the aggregation process is only studied as a function of time for different external field strength or concentration of the colloidal system [13,23,26,28–34,36–43,48–50]. But the influence of external field exposure time and viscous force that competes with the one arising from dipolar interaction between the magnetic particles is not systematically studied. When the size of magnetic colloidal particles are in the nanorange ($a < 5$ nm); the challenge in studying aggregation kinetics under external field increases manifold because of the limited experimental

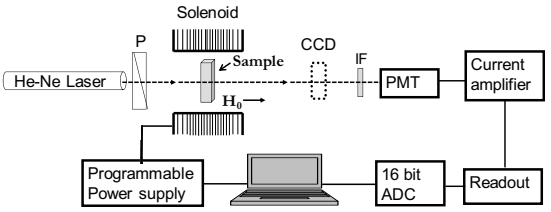

FIG. 1. Schematic of the experimental setup. The direction of the applied magnetic field is along the direction of propagation of the beam. P-polarizer and IF-interference filter.

tools and the requirement of nanoparticles dispersions with good monodispersity and stability. We have shown that the variation of the transmitted light intensity and scattered pattern is a measure of the field induced aggregation process [45]. In ionic ferrofluids, the electrostatic interaction plays a major role in the aggregation process and aggregated structures are irreversible at high field strength. To avoid complexities originating from the electrostatic interactions, we chose a nonaqueous nanofluid of Fe_3O_4 nanoparticles for our study [51]. Due to steric stabilization, the aggregation process is perfectly reversible on removal of magnetic field and the system goes back to initial dispersed condition. In this paper, using light scattering technique, we study the kinetics of aggregation and deaggregation in a stable dispersion of iron oxide nanoparticles by systematically varying the ramp rate of the applied magnetic field.

II. MATERIAL AND EXPERIMENTAL METHOD

The experiments are performed in a stable colloidal system of magnetite (Fe_3O_4) particles coated with oleic acid and dispersed in a hydrocarbon carrier fluid. Average diameter of the particles and organic layer thickness around the particles are 6.5 and 1.5 nm, respectively. We eliminate the complexities originating from electrostatic interactions between the nanoparticles by using a nonaqueous nanofluid. Transmitted light intensity and the scattered pattern are acquired as a function of magnetic field to study the aggregation process using a fully automated light scattering setup shown in Fig. 1. An amplitude and frequency stabilized polarized He-Ne laser (spectra-physics) of wavelength (λ) 632.8 nm with an output power 1 mW is used as a light source. The propagation wave vector of incident light is parallel to the external field direction. To study the influence of rate of increase in the external field on the aggregation kinetics, the transmitted light and scattered patterns are acquired at different ramp rates. Ramp rate of the applied field is varied by using a programmable current source and a solenoid, in which the sample is placed in a sealed a quartz cuvette. Transmitted light intensity is measured using a photomultiplier tube (PMT Oriel) and its output is fed to readout through a current amplifier with variable gain. The analog output from the readout is connected to a 16 bit analog-to-digital converter (ADC) that is interfaced with a computer. The scattered pattern, observed on a screen is recorded using a charge-coupled device (CCD) camera.

III. THEORETICAL BACKGROUND

The nanoparticles in magnetic colloids are in random thermal Brownian motion in the absence of external mag-

netic field. On application of external magnetic field, each individual particle acquire dipole moment of the magnitude given by

$$m = \frac{4}{3}\pi a^3 \chi H_0, \tag{2}$$

where a the radius of the particle is, χ is the magnetic susceptibility and H_0 is the magnitude of external magnetic field. This causes the moments of the particles to align along the field direction and also increases the anisotropic interaction energy between two such particles, given by [19]

$$U_{ij}(r_{ij}, \theta_{ij}) = \frac{m^2 \mu_0}{4\pi}\left(\frac{1 - 3\cos^2\theta_{ij}}{r_{ij}^3}\right), \tag{3}$$

where r_{ij} is the position vector of ith particle relative to the jth particle and θ_{ij} is the angle between the external field and the position vector. As the particles are in Brownian motion, the effective interaction between them can be described by a coupling constant ($\wedge$) which is the ratio of the maximum magnitude interaction energy to the thermal energy ($k_B T$) in the system

$$\Lambda = \frac{\pi \mu_0 d^3 \chi^2 H_0^2}{72 k_B T}. \tag{4}$$

Here, k_B is the Boltzmann constant, T is the temperature and d is the diameter of the particle. When $\wedge \geq 1$, the particles in the dispersion self-assemble to form one dimensional chain like structures along the field direction. Magnetic force between two particles having induced moment m is given by

$$F = -\nabla U. \tag{5}$$

Initial time (t_c) for two particles to aggregate is derived using the magnetic potential given by Eq. (2), Stokes drag law and Eq. (4) and is given as [52]

$$t_c = \frac{a}{5}\frac{6\pi a \eta}{F_{\max}}\left[\left(\frac{r}{2a}\right)^5 - 1\right]. \tag{6}$$

Where magnetic force between particles at contact is given by $F_{\max} = \frac{\mu_0}{4\pi}\frac{3m^2}{8a^4}$, r is the initial separation distance between the particles and η is the viscosity of the carrier liquid. The initial separation distance r between two particles is considered as the average antiparticle spacing for a given concentration. Considering the particles as spherical, the interparticle spacing (IPS) for a colloidal dispersion of monodisperse particles is given by [53]

$$IPS = 2a\left[\left(\frac{\phi_m}{\phi}\right)^{1/3} - 1\right]. \tag{7}$$

Where ϕ is the particle volume fraction and ϕ_m is the maximum particle packing fraction which is 0.63 for random dense packing.

IV. RESULTS AND DISCUSSIONS

Figure 2 shows the variation of normalized transmitted intensity when the magnetic field is increased at different ramp rates for a dispersion of volume fraction (ϕ) 0.006 49. For all rates, the transmitted intensity decreases with the increase in magnetic field. For the slowest ramp rate i.e., 0.6 G/s, the rate of decay in transmitted intensity is also slow. On increasing the ramp rate, the transmitted intensity decays faster. When the rate is increased further, i.e., above 2.5 G/s, the transmitted intensity shows a reverse trend with a slower decay of transmitted intensity with decrease in field. Figure 2(B) shows that the higher the ramp rate the slower is the rate of decrease of transmitted intensity. Another important observation from the Figs. 2(A) and 2(B) is that all the curves overlap each other up to a magnetic field of 70 G, above which the slope of transmitted intensity curves differs.

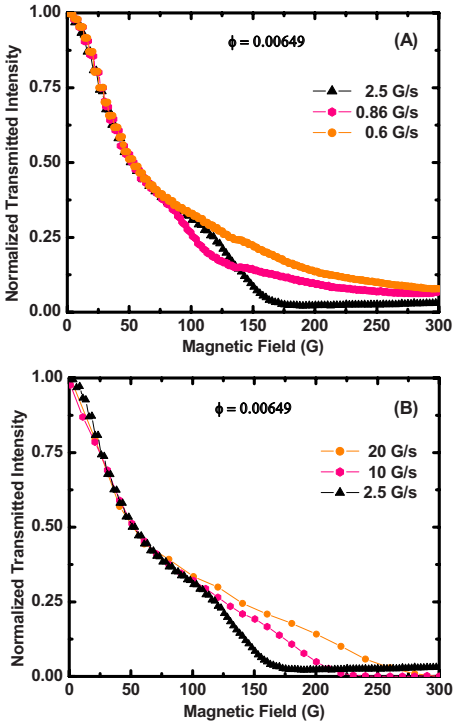

FIG. 2. (Color online) Normalized transmitted spot intensity as function of the external magnetic field (during increase) for different ramp rates for volume fraction $\varnothing = 0.006\,49$ of Fe_3O_4.

The scattered patterns at four different magnetic fields of 0, 150, 250, and 300 G, for three different ramp rates of 0.6, 10, and 20 G/s are shown in Fig. 3. In the absence of any field, only a diffused spot is observed for all the ramp rates. But as the field is increased, the observed scattered patterns show different features. Figure 3(A)–3(D) shows the scattered pattern for a ramp rate of 0.6 G/s. As the field increases, the spot is transformed to a diffused plume which in turn changes to a diffused ring with the transmitted light spot appearing on the circumference of the ring at high-magnetic field. Since the chain like structures are formed along the field direction, the reason for the formation of ring structure on the scattered pattern can be explained by considering scattering of light by a cylinder [45,54]. The observed pattern can be understood by evaluating the scattered electromagnetic field when an infinite right circular cylinder of radius a is illuminated by a plane homogeneous wave $\mathbf{E}_i = \mathbf{E}_0 e^{ik\hat{\mathbf{e}}_i \cdot \mathbf{x}}$ propagating in the direction $\hat{\mathbf{e}}_i = -\sin\zeta\hat{\mathbf{e}}_x - \cos\zeta\hat{\mathbf{e}}_z$, where ζ is

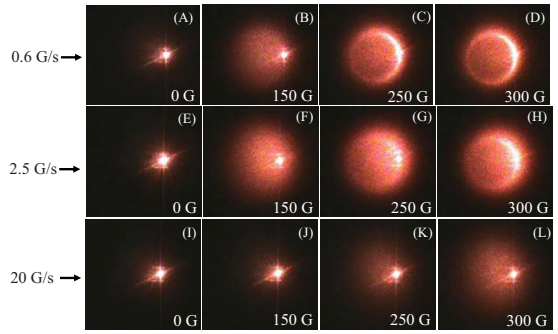

FIG. 3. (Color online) Light Scattered patterns at different magnetic field values (during increase) on a screen placed perpendicular to the field direction of incident light for ramp rates 0.6 G/s (A-D), 2.5 G/s (E-H), and 20 G/s (I-L).

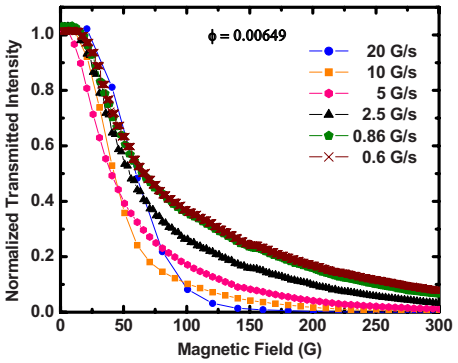

FIG. 4. (Color online) Normalized transmitted spot intensity as function of the external magnetic field (during decrease) at different ramp rates for volume fraction $\varnothing = 0.006\,49$ of Fe_3O_4.

the angle between the incident wave and the cylinder axis. It is inferred from the derived expressions of scattered field that the surfaces of constant phase, or wave fronts, of the scattered wave are the points which satisfy

$$f(x,y,z) = r \sin \zeta - z \cos \zeta = C. \tag{8}$$

Therefore, the wave fronts are cones of half-angle ζ with their apexes at

$$z = -\frac{C}{\cos \zeta}. \tag{9}$$

The propagation of the scattered wave can be visualized as a cone that is sliding down the cylinder. The direction of propagation at any point on the cone, or wave normal $\hat{\mathbf{e}}_\mathbf{S}$ is

$$\hat{\mathbf{e}}_\mathbf{s} = \nabla f = \sin \zeta \hat{\mathbf{e}}_\mathbf{r} - \cos \zeta \widehat{\mathbf{e}_\mathbf{z}}. \tag{10}$$

The Poynting vector is therefore, in the direction $\hat{\mathbf{e}}_\mathbf{S}$.

It is clear from Eqs. (9) and (10) that if a screen perpendicular to the incident beam, is placed at some distance from the cylinder, the resulting scattered patterns that form on the screen will be cross section of cones or conic sections. When light is incident at zero degree to the cylinder axis ($\zeta = 0°$), the scattered pattern is a circle. For angles of incidence less than 45°, ellipses appear on the screen. At 45° the pattern is a parabola and for more than 45°, the succession of hyperbolas is traced out. When the incident light is normal to the cylinder axis, the pattern becomes a straight line. The formation of the ring clearly establishes the formation of such chainlike structures along the direction of propagation of the light when the coupling constant $\Lambda \geq 1$.

Sharpness of the ring increases as the external field is increased and reaches its maximum at high field value. When the field is increased at a higher ramp rate of 2.5 G/s, the diffused plume of scattered light is again formed at an intermediate field value but with higher intensity as shown in Figs. 3(F) and 3(G). At these intermediate fields (i.e., 150–250 G); the spot on the circumference was less intense compared to the previous rate (0.6 G/s) that is also evident from the corresponding intensity curves in Fig. 2(A). Hardly any change is observed in the intermediate fields when the ramp rate is very high i.e., 20 G/s. Here, no ring structure in the scattered pattern is formed even at high field strength. Only a diffused plume with less brightness is seen [Fig. 3(L)].

After increasing the magnetic field at a particular ramp rate to the highest value i.e., 300 G, the field is again decreased to the lowest value i.e., 0 G with the same ramp rate. This is repeated for three different ramp rates of 0.6, 10, and 20 G/s. Figure 4 shows the variation of transmitted intensity as a function of magnetic field for different ramp rates during the decrease in the field. It is observed that the transmitted intensity increases with the decrease in the magnetic field for all ramp rates. When the ramp rate is very high i.e., 20 G/s, the transmitted intensity starts to rise sharply as the magnetic field is decreased below 100 G. As the ramp rate is lowered, the rise in the transmitted intensity with decrease in the field becomes smoother. For lower ramp rate during the decrease in the field, the transmitted intensity rise is faster. There is not much variation in the transmitted intensity when the ramp rate is below 0.86 G/s. Another important observation is that the transmitted intensity is maximum for the entire magnetic field range for the lowest rate i.e., 0.6 G/s.

The scattered patterns and their corresponding surface plots at different magnetic field values (during decrease) for three different ramp rates are shown in Fig. 5 for comparison. For all ramp rates, on decreasing the magnetic field to zero value, the scattered pattern finally goes back to the original diffused spot, indicating the perfect reversibility of the aggregation process. Figures 5(A)–5(D) and 5(M)–5(P) shows that the sharpness of the ring structure in the scattered pattern is maximum at 250 G, when the field is decreased at a ramp rate of 0.6 G/s. With further decrease in the field, the sharpness of the ring is also decreased (150 and 50 G). Especially, the left half of the ring diminishes and a diffused spot appears as the field is reduced to zero. Similar transformation of ring like structure to a diffused spot is observed when the field is dropped to zero at a ramp rate of 2.5 G/s as seen in Figs. 5(E)–5(H) and 5(Q)–5(T). When the field is decreased at a faster rate of 20 G/s, a bright diffused circular plume of scattered light is observed at 250 G. On further decrease in the field, both spot and total brightness of the plume is decreased and finally transformed into a diffused spot at zero fields. At the same time the transmitted spot becomes brighter with the decrease in the magnetic field, which is also evident in the intensity variation curve in Fig. 4.

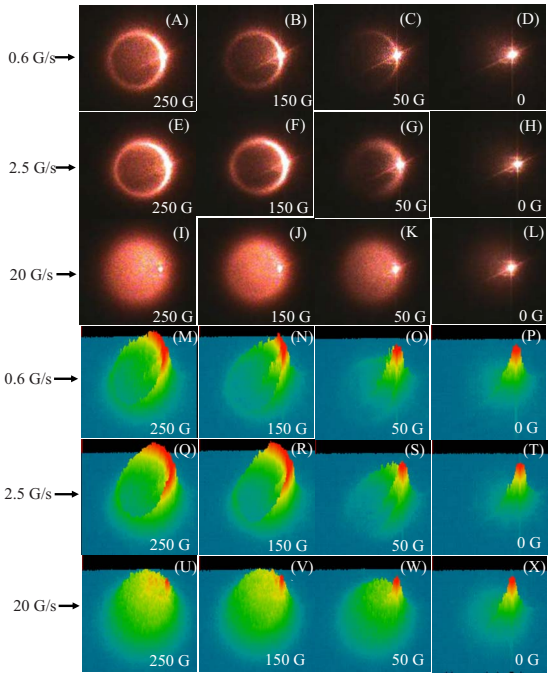

FIG. 5. (Color online) Light Scattering patterns from the nanofluid at different magnetic field values (during decrease) on a screen placed perpendicular to the field direction of incident light and their corresponding surface plots for ramp rates 0.6 G/s (A-D and M-P), 2.5 G/s (E-H and Q-T), and 20 G/s (I-L and U-X).

Figure 6 shows the variation of transmitted intensity for two different ramp rates as a function of magnetic field, both during its increase and decrease. For the faster ramp rate i.e., 20 G/s, a large hysteresis in the transmitted intensity curves are observed during the increase and decrease of magnetic field. However, for a slow rate of 0.6 G/s, no hysteresis is observed during decrease and increase in the applied magnetic field. Now, to have a better idea about the reversibility of the aggregation process for different ramp rates, the area of the gap between the two curves is calculated. This gap area is an indicator of the reversibility of the aggregation process and is defined as the hysteresis area. It is found that the hysteresis area increases with the increase in the ramp rate in a linear fashion as shown in Fig. 7. It shows that hysteresis is large at higher ramp rates compared to the lower ones, indicating that the irreversibility of field induced aggregates increases with the increase in the ramp rate. These observations show that ramp rate of external magnetic field plays an important influence in the aggregation and deaggregation process. The aggregation rate increases on increasing the ramp rate up to an optimum rate (2.5 G/s). But, on further increase of the ramp rate from 2.5 G/s, the rate of aggregation of the particles becomes slower.

Now, considering the system as a light scattering media, the size of scatterers actually increases as the particles start forming doublets, triplets and chains along field direction when the coupling constant, $\Lambda \geq 1$ as given by Eq. (4) on increasing the field. This increase in the scatterers' size can lead to the occurrence of resonance in the scattering efficiency [55]. Diffused plume of scattered light accompanied by a decrease in the transmitted spot intensity (Figs. 2 and 3)

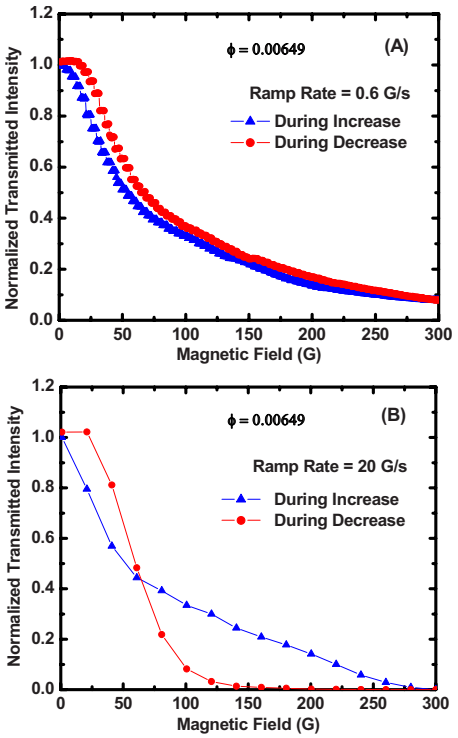

FIG. 6. (Color online) Normalized transmitted spot intensity as function of the external magnetic field (during increase and decrease) for volume fraction $\varnothing = 0.006\,49$ of Fe_3O_4 at the ramp rate of 0.6 G/s (A) and 20 G/s (B).

is due to the enhancement in the amount of light scattering. The type of the scattered pattern, its brightness and the transmitted spot intensity depends on the number, size, shape and distribution of the scatterers. After the formation of chains, the zippering of chains take place due to the lateral aggregation to reach the equilibrium structure if the system gets sufficient time [15,19,20,48]. The observation of the variation of light transmission and the scattered pattern with ramp rate clearly indicates that the number, size, shape and the distribution of the field induced aggregates are not the same even for the same field if the ramp rates are different.

The transmitted light through a dispersion of slab length L is given by

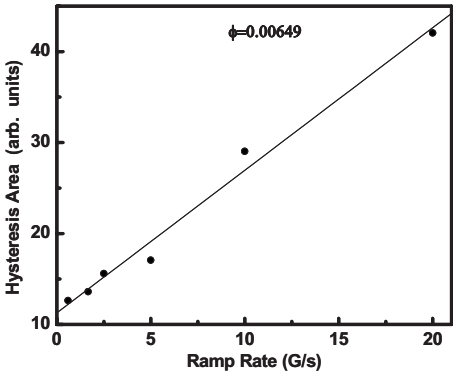

FIG. 7. Hysteresis area of the transmitted light intensity curve as function of the ramp rate of external field for volume fraction $\varnothing = 0.006\,49$ of Fe_3O_4.

$$I_t = I_0 \exp(-\alpha_{ext} L). \tag{11}$$

Where I_0 is the incident light intensity, I_t is the transmitted intensity, $\alpha_{ext}(=nC_{ext})$ is the extinction coefficient, $n(=\frac{4}{3}\pi a^3 \phi)$ is the number of particles per unit volume, ϕ is the particle volume fraction, $C_{ext}(=\pi a^2 Q_{ext})$ is the extinction cross section of the particles due to light scattering and Q_{ext} is the extinction efficiency. The extinction of light while propagating through the dispersion of magnetic particles is due to both absorption and scattering of light. Therefore, the total attenuation is due to the combined effect of absorption and scattering of light by the dispersed magnetic particles for a given path length. It should be noted that in our case the path length (L) is 1 mm for which the attenuation is 73% at 632 nm. In the dilute regime ($\phi < 0.01$), multiple scattering can be neglected [56] and in our case ϕ was 0.006 49. According to Born approximation, the weak scattering condition is $kl > 1$ where $k(=2\pi N/\lambda)$ wave vector is and $l(=2d/3\phi Q_{ext})$ is the scattering mean free path [56,57]. Here, N is the refractive index of carrier liquid, d is particle diameter. Scattering extinction efficiency (Q_{ext}) is calculated using Mie theory [54]. Since $kl \sim 9.5 \times 10^5$ in our case, contribution from multiple scattering can be ignored. Studies in Fe_3O_4 nanoparticle dispersion in kerosene show very little absorption at 632 nm [58]. When $a \ll \lambda$, there is substantial decrease in transmitted intensity when aggregation occurs and this aspect has been exploited to measure relative coagulation rates and stability ratios [59]. By correlating transmitted intensity (I_t) with scattering efficiency (Q_{ext}), the aggregate size can be found [60,61]. However, in our case the size of aggregates increases linearly. The shape of the linear aggregates at different fields is no longer spherical but cylindrical.

The finite cylinder scattering problem is not exactly solvable, only analytical expressions can be obtained for amplitude scattering matrix elements in the Rayleigh-Gans approximations [54]. Since, the condition $|m-1| \ll 1$ for Rayleigh-Gans approximations is not satisfied, the above solution is not valid for our system (refractive index, m=2.33776 for Fe_3O_4). Using a numerical method, called volume integral equation formalism (VIEF), the scattering efficiency is evaluated for finite cylinder when the incident radiation falls along the axis of the cylinder [62]. It is shown that for a given diameter and refractive index of the cylinder, the scattering efficiency increases as cylinder length is increased in the low-wave number limit of visible range. Thus, the basic underlying mechanism for the decrease in transmitted intensity is the enhancement in light scattering due to the increase in length of the cylindrical aggregates.

Depending on three transport mechanisms, different aggregation mechanisms are defined. These are (1) *perikinetic* aggregation arising from Brownian diffusion, (2) *orthokinetic* aggregation arising from fluid motion, and (3) *differential sedimentation* arising from settling of particles of different size or density from a suspension [63]. Aggregation times are estimated for various colloidal systems considering these aggregation mechanisms [44]. All the above mentioned aggregation times refer to time scales for irreversible macroscopic aggregation e.g., visible sedimentation or gelation which takes place in unstable colloidal systems.

Unlike the above mentioned mechanisms, the aggregation process is perfectly reversible in the present system as the system goes back to the initial condition upon removal of magnetic field. This is evident from the regaining of the transmitted intensity to its original value upon removal of the magnetic field as shown in Figs. 4 and 6.

On the application of external field, the magnetization of the particles dispersed in the carrier liquid can relax by two mechanisms. First, the relaxation occurs by particle rotation in the liquid known as the Brownian relaxation with a rotational diffusion time given by [64–66]

$$\tau_B = 3V_h \eta / k_B T, \tag{12}$$

where V_h is the hydrodynamic particle volume. Second, the relaxation is due to rotation of magnetic vector within the particle known by Neel relaxation mechanism with a characteristic time given by

$$\tau_N = \frac{1}{f_0} \exp\left(\frac{KV_m}{k_B T}\right) \Bigg/ \left(\frac{KV_m}{k_B T}\right)^{-1/2} \quad \frac{KV_m}{k_B T} > 2 \tag{13}$$

$$\cong \frac{1}{f_0} \exp\left(\frac{KV_m}{k_B T}\right) \quad \frac{KV_m}{k_B T} \ll 1, \tag{14}$$

where f_0 is the attempt frequency, K is the anisotropy constant of the material and V_m is the magnetic volume of the particle. Considering the parameters $f_0 = 10^9$ Hz, $K = 44$ kJ/m^3, $\eta = 0.002$ kg m^{-1} s^{-1} for kerosene, the magnetic diameter $d_m = 6.5$ nm and the hydrodynamic diameter $d_h = d_m + 2s$ where $s = 1.5$ nm being the polymeric surface layer thickness; the Brownian and Neel relaxation times for our system are found to be 7.12×10^{-7} and 4.12×10^{-9} sec, respectively. Since these time scales are much faster compared to our experimental observations, any role of these kinds of relaxation processes on the decrease of transmitted intensity i.e., on the rate of field induced aggregation process can be safely ruled out.

The time required for aggregation of the particles and linear aggregates in a carrier liquid for a given external field depends on two competing forces experienced by them: First, the magnetic force due to field induced magnetic moment and second, the viscous force. The magnetic force depends on the particle size, number of particles in linear aggregates and external field strength whereas the viscous force depends on the particle or aggregate size and viscosity of the carrier liquid. Therefore, for a given sample concentration the aggregation time changes with the external field strength. To obtain better insight into the nature of this variation i.e., the kinetics of the field induced aggregation process, the initial aggregation time between the colloidal magnetic particles are estimated for different fields using Eq. (6) by considering the parameters of the experimental system i.e., the particle radius $a = 3.25$ nm, viscosity of the carrier liquid i.e., kerosene $\eta = 0.002$ kg m^{-1} s^{-1}, magnetic permeability $\mu = 1.2566 \times 10^{-6}$ TmA^{-1}. The initial separation distances r required for the above calculation are found using Eq. (7) to be 107.02, 72.57, 54.47 and 46.11 nm for 0.003 19, 0.006 49,

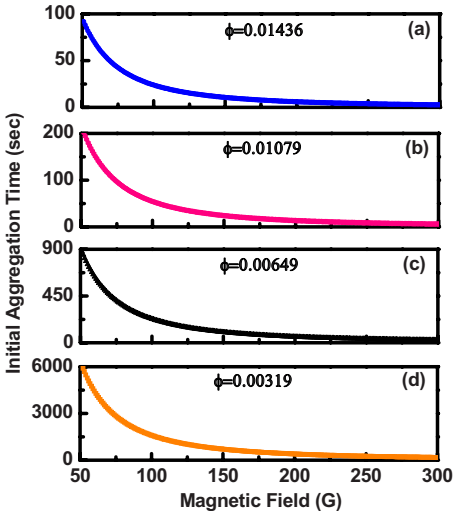

FIG. 8. (Color online) Initial aggregation time between two magnetic particles in dispersion as function of external magnetic field for sample of volume fractions ($\varnothing$) (a) 0.014 36, (b) 0.010 79, (c) 0.006 49, and (d) 0.003 19.

0.010 79, and 0.014 36 volume fractions of the sample respectively. The magnetic field dependence of the aggregation time for two spherical particles is shown in Figs. 8 and 9. In the present system, even though at zero or at very low fields, there were only spherical particles; once they start forming doublets, triplets and chains, the length of the aggregates increases and also their shape can be considered similar to cylinders. With the increase in magnetic field, the shape, size, and the aggregate separation changes. This results in changes in the aggregation time too. To get the exact aggregation time for a given field, the viscous force of two cylindrical aggregates of given lengths and separation should be balanced with the magnetic force. The major contributing term that affects the aggregation time scale in Eq. (6) is $\frac{r}{2a}$ i.e., the ratio of particle or aggregate separation distance (r)

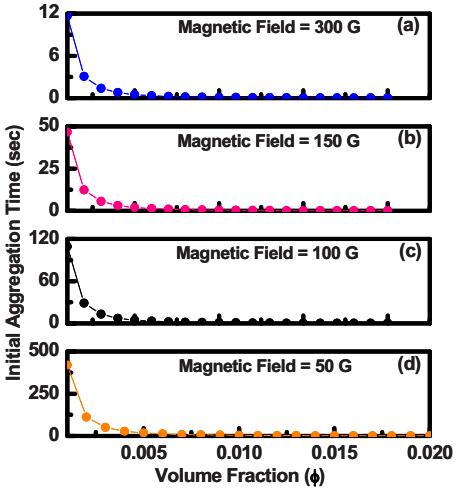

FIG. 9. (Color online) Initial aggregation time between two magnetic particles in a dispersion as function of volume fraction for external magnetic field (H_0) values (a) 300 G (b) 150 G (c) 100 G, and (d) 50 G.

and their size (here diameter $2a$). With the increase in size i.e., length of the linear aggregates, their separation distance also increases thereby keeping the ratio $\frac{r}{2a}$ more or less the same. There is no reason for the other terms to affect the aggregation time significantly under the changing spatial and geometrical scenario inside the system upon increasing the field. Therefore, Eq. (6) can be considered to give a good estimate of the time scale of aggregation between the aggregates and its variation with magnetic field.

Figure 8 shows that the aggregation time decreases with the increase in magnetic field, as magnetic force experienced by the aggregates dominates the viscous force at higher field values. Changing the ramp rate actually changes the time for which the particles and the aggregates are exposed to different external field values during the increase in the field. The exposure time should be at least equal to the aggregation time so that the aggregates can attain their maximum permissible length for any given field strength. Aggregation rate is very high when the exposure time is equal to the aggregation time but decreases when the exposure time is either more or less than the aggregation time.

For sample volume fraction $\varnothing$=0.006 49, aggregation time is 400 s for external field H_0=75 G that decreases to 25 s for H_0=300 G as shown in Fig. 8(c).When the external field is ramped from 0 to 300 G at 20 G/s, the total available exposure time for the sample is 15 s which is even less than the aggregation time for H_0=300 G. Therefore, the aggregates cannot reach their permissible length. When the external field is increased from 0 to 300 G at a very slow ramp rate of 0.6 G/s, the total exposure time for the sample is 500 s which is more than that required for the aggregates to reach their permissible lengths. Due to the delay in reaching the higher field values, the aggregation rate decreases again that is evident from slow increase in transmitted intensity for 0.6 G/s [Fig. 2(A)]. Therefore, there exists an optimum ramp rate for which the exposure time just equals the aggregation time. At this optimum ramp rate the aggregates reach their permissible lengths in minimum time to cause fastest decrease of transmitted intensity. For the present system, fastest aggregation i.e., fastest decrease of transmitted intensity occurs for the ramp rate of 2.5 G/s [Figs. 2(A) and 2(B)]. Therefore, for sample volume fraction $\varnothing$=0.006 49, the aggregation time is 120 s as this corresponds to an optimum ramp rate of 2.5 G/s (for 0 to 300G). Interestingly, this time scale matches fairly well with the reported values of the characteristic time scales for the two competing processes-field-induced cluster formation and thermally activated dissociation, which is found to be 100 to 150 s for an ionic ferrofluid measured from the variation of Raman intensity on applying external magnetic field of 150 G [40]. Therefore, the interplay between the aggregation time and the exposure time for a given volume fraction explains the nonmonotonic variation in the transmitted light intensity. Also, the increase in sharpness and clarity of the ring structure formed in the scattered pattern [Fig. 3] at low-ramp rates confirms that at higher fields the particles and aggregates in the dispersion have sufficient time to increase the length and arrange themselves.

Also, the deaggregation time also depends on external field strength. For slow ramp rate (0.6 G/s), exposure time is more than that required for both aggregation and deaggrega-

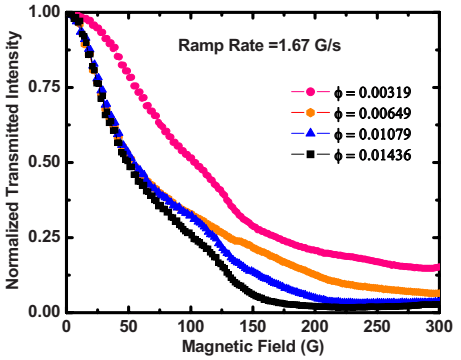

FIG. 10. (Color online) Normalized transmitted spot intensity as function of the external magnetic field (during increase) at a ramp rate of 1.67 G/s for different volume fractions of Fe_3O_4.

tion. The aggregates are of same lengths at a given field, both during the increase and decrease as they reach their maximum value. This leads to the same intensity value for the two curves at different fields making them nearly overlap each other. The area between the transmitted intensity curves during "increase" and "decrease" for a given ramp rate is defined as the Hysteresis area. Physically, this hysteresis area gives an indication whether the aggregate size is same at a given external field during its increase and decrease for a particular ramp rate. In other words, this describes the reversibility of the aggregation process for a given ramp rate. The Hysteresis area is very less for slow ramp rate of 0.6 G/s [Fig. 6(A)].

For fast ramp rate (20 G/s), exposure time is much less than that required for both aggregation and deaggregation. Since the aggregates cannot reach their permissible lengths, the transmitted intensity decreases slowly during the increase in field [Figs. 2(A) and 6(B)]. Again, during the decrease in field, the aggregates get very less time to decrease their length sufficiently until the magnetic field strength of 150 G [Figs. 4 and 6(B)]. But, on further decrease in field, the magnetic force between the aggregates becomes very weak to retain the linear aggregates intact and the thermal energy due to Brownian motion dominates the dipolar interaction energy of the particles and aggregates. Since, the deaggregation takes place very fast after lowering the field below 150 G, the transmitted intensity suddenly shoots up and also intersects the intensity curve that is obtained during increase in field. This results in two distinct areas in the hysteresis curve as shown in Fig. 6(B). Also, for low-ramp rates the decrease in chain length by deaggregation takes place in an ordered fashion and chain structure is retained even at very low field that is evident from the partial ring in the scattered patterns [Figs. 5(B) and 5(C)]. Faster deaggregation at higher ramp rates results in linear aggregates that are randomly ordered. Scattering from these disordered linear aggregates results in the diffused plume as shown in Figs. 5(J) and 5(K).

Figure 9 shows the initial aggregation time between two magnetic particles in dispersion as function of ϕ for four external magnetic field values of 50, 100, 150, and 300 G. To check the dependence of initial aggregation time on the concentration of sample as shown in Figs. 8 and 9, the transmitted intensity is measured and plotted in Fig. 10. The ϕ values were 0.003 19, 0.006 49, 0.010 79, and 0.014 36 and the external field is increased at the same ramp rate of 1.67 G/s. The transmitted intensity is found to decay faster as the ϕ of the sample increases. Similar observation is seen on increasing the external field at other ramp rates. For the same applied field, the initial aggregation time is less for higher concentrations due to smaller interparticle separation distance. This rapid formation of field induced linear chainlike structures results in faster decay of transmitted intensity in samples with high ϕ.

V. CONCLUSION

The role of external applied field ramp rate on the rate of formation of linear aggregation in magnetic nanoparticles dispersion is studied from transmitted intensity and scattered pattern. The transmitted intensity decay rate increases with ramp rate, but the trend became reversed above an optimum ramp rate. Calculation of initial aggregation time as a function of magnetic field shows that, for ϕ=0.006 49 an optimal ramp rate of 2.5 G/s is necessary to complete the initial aggregation process where decay of transmitted intensity is fastest. For faster ramp rate, insufficient exposure time results in the slow decay of transmitted intensity. The rate of deaggregation of the field induced linear structures into dispersion is found to be dependent on the ramp rate at which external magnetic field is decreased. The requirement of a minimum time for deaggregation is evident from the change in the slope of the transmitted intensity curves during the decrease in the field. The observed scattered patterns for different ramp rates show the evolution of field induced structures during aggregation and deaggregation under external field. Disappearance of the ring pattern and the reappearance of original spot, upon removal of the magnetic field, confirm the perfect reversibility of the aggregation process. The hysteresis in the aggregation process is found to decrease with the increase in the ramp rate. The change in the decay rate with the volume fraction of the nanoparticles is consistent with particle aggregation theory.

ACKNOWLEDGMENT

Authors express their sincere thanks to Dr. T. Jayakumar for fruitful discussions.

[1] M. Y. Lin, H. M. Lindsay, D. A. Weitz, R. C. Ball, R. Klein, and P. Meakin, Nature (London) **339**, 360 (1989).
[2] P. C. Hiemenz and R. Rajagopalan, *Principles of Colloid and Surface Chemistry* (Dekker, New York, 1997).
[3] J. Philip, P. D. Shima, and B. Raj, Appl. Phys. Lett. **92**, 043108 (2008).
[4] P. D. Shima, J. Philip, and B. Raj, Appl. Phys. Lett. **95**, 133112 (2009).
[5] V. Cabuil, *Preparation and Properties of Magnetic Nanoparticles, Encyclopedia of Surface and Colloid Science* (Dekker, New York, 2004).
[6] J. Philip, T. Jaykumar, P. Kalyanasundaram, and B. Raj, Meas. Sci. Technol. **14**, 1289 (2003).
[7] H. E. Horng, C. S. Chen, K. L. Fang, S. Y. Yang, J. J. Chieh, C.-Y. Hong, and H. C. Yang, Appl. Phys. Lett. **85**, 5592 (2004).
[8] J. J. Chieh, S. Y. Yang, H. E. Horng, C.-Y. Hong, and H. C. Yang, Appl. Phys. Lett. **90**, 133505 (2007).
[9] A. F. Bakuzis, K. S. Neto, P. P. Gravina, L. C. Figueiredo, P. C. Moraisa, L. P. Silva, R. B. Azevedo, and O. Silva, Appl. Phys. Lett. **84**, 2355 (2004).
[10] J. Philip, G. Prakash, T. Jayakumar, P. Kalynasundaram, and B. Raj, Phys. Rev. Lett. **89**, 268301 (2002).
[11] J. Liu, E. M. Lawrence, A. Wu, M. L. Ivey, G. A. Flores, K. Javier, J. Bibette, and J. Richard, Phys. Rev. Lett. **74**, 2828 (1995).
[12] G. A. Flores, J. Liu, M. Mohebi, and N. Jamasbi, Phys. Rev. E **59**, 751 (1999).
[13] M. Fermigier and A. P. Gast, J. Colloid Interface Sci. **154**, 522 (1992).
[14] D. Wirtz and M. Fermigier, Phys. Rev. Lett. **72**, 2294 (1994).
[15] E. M. Furst and A. P. Gast, Phys. Rev. E **62**, 6916 (2000).
[16] A. J. Dickstein, S. Erramilli, R. E. Goldstein, D. P. Jackson, and S. A. Langer, Science **261**, 1012 (1993).
[17] R. M. Erb, H. S. Son, B. Samanta, V. M. Rotello, and B. B. Yellen, Nature (London) **457**, 999 (2009).
[18] M. F. Islam, K. H. Lin, D. Lacoste, T. C. Lubensky, and A. G. Yodh, Phys. Rev. E **67**, 021402 (2003).
[19] R. Haghgooie and P. S. Doyle, Phys. Rev. E **75**, 061406 (2007).
[20] J. M. Laskar, J. Philip, and B. Raj, Phys. Rev. E **80**, 041401 (2009).
[21] M. Ivey, J. Liu, Y. Zhu, and S. Cutillas, Phys. Rev. E **63**, 011403 (2000).
[22] M. Klokkenburg, B. H. Erne´, J. D. Meeldijk, and A. Wiedenmann, Phys. Rev. Lett. **97**, 185702 (2006).
[23] J. Promislow, A. P. Gast, and M. Fermigier, J. Chem. Phys. **102**, 5492 (1995).
[24] H. Zhang and M. Widom, Phys. Rev. E **51**, 2099 (1995).
[25] S. Miyazima, P. Meakin, and F. Family, Phys. Rev. A **36**, 1421 (1987).
[26] G. Helgesen, A. T. Skjeltorp, P. M. Mors, R. Botet, and R. Jullien, Phys. Rev. Lett. **61**, 1736 (1988).
[27] T. Vicsek and F. Family, Phys. Rev. Lett. **52**, 1669 (1984).
[28] M. C. Miguel and R. Pasto-Satorras, Phys. Rev. E **59**, 826 (1999).
[29] G. Bossis, C. Mathis, Z. Minouni, and C. Paparoditis, EPL **11**, 133 (1990).
[30] D. Sohn, J. Magn. Magn. Mater. **173**, 305 (1997).
[31] J. Cernak, P. Macko, and M. Kasparkova, J. Phys. D **24**, 1609 (1991).
[32] J. Cernak, J. Magn. Magn. Mater. **132**, 258 (1994).
[33] J. E. Martin, J. Odinek, and T. C. Halsey, Phys. Rev. Lett. **69**, 1524 (1992).
[34] S. Melle, M. A. Rubio, and G. G. Fuller, Phys. Rev. Lett. **87**, 115501 (2001).
[35] R. M. Erb, M. D. Krebs, E. Alsberg, B. Samanta, V. M. Rotello, and B. B. Yellen, Phys. Rev. E **80**, 051402 (2009).
[36] P. D. Duncan and P. J. Camp, J. Chem. Phys. **121**, 11322 (2004).
[37] P. D. Duncan and P. J. Camp, Phys. Rev. Lett. **97**, 107202 (2006).
[38] T. Ukai and T. Maekawa, Phys. Rev. E **69**, 032501 (2004).
[39] M. Mohebi, N. Jamasbi, and J. Liu, Phys. Rev. E **54**, 5407 (1996).
[40] D. Heinrich, A. R. Goni, and C. Thomsen, J. Chem. Phys. **126**, 124701 (2007).
[41] F. Martínez-Pedrero, A. El-Harrak, J. C. Fernandez-Tolenado, M. Tirado-Miranda, J. Baudry, A. Schmitt, J. Bibette, and J. C. Fernandez, Phys. Rev. E **78**, 011403 (2008).
[42] F. Martínez-Pedredo, M. T. Miranda, A. Schmitt, and J. C. Fernandez, J. Chem. Phys. **125**, 084706 (2006).
[43] A. Wiedenmann, U. Keiderling, K. Habicht, M. Russina, and R. Gahler, Phys. Rev. Lett. **97**, 057202 (2006).
[44] L. G. B. Bremer, P. Walstra, and T. v. Vliet, Colloids Surf., A **99**, 121 (1995).
[45] J. M. Laskar, J. Philip, and B. Raj, Phys. Rev. E **78**, 031404 (2008).
[46] C.-Y. Hong, C.-H. Lin, C.-H. Chen, Y. P. Chiu, S. Y. Yang, H. E. Horng, and H. C. Yang, J. Magn. Magn. Mater. **226-230**, 1881 (2001).
[47] H. E. Horng, C.-Y. Hong, S. Y. Yang, and H. C. Yang, J. Phys. Chem. Solids **62**, 1749 (2001).
[48] C. Rablau, P. Vaishnava, C. Sudakar, R. Tackett, G. Lawes, and R. Naik, Phys. Rev. E **78**, 051502 (2008).
[49] W. D. Young and D. C. Prieve, Ind. Eng. Chem. Res. **35**, 3186 (1996).
[50] J. J. M. Janssen, J. J. M. Baltussen, A. P. v. Gelder, and J. A. A. J. Prenboom, J. Phys. D **23**, 1447 (1990).
[51] G. Gnanaprakash, J. Philip, T. Jayakumar, and B. Raj, J. Phys. Chem. B **111**, 7978 (2007).
[52] D. Liu, M. R. Maxey, and G. E. Karniadakis, J. Micromech. Microeng. **15**, 2298 (2005).
[53] T. Hao and R. E. Riman, J. Colloid Interface Sci. **297**, 374 (2006).
[54] C. F. Bohren and D. R. Huffman, *Absorption and Scattering of Light by Small Particles* (Wiley-Interscience, New York, 1983).
[55] F. A. Pinheiro, A. S. Martinez, and L. C. Sampaio, Phys. Rev. Lett. **84**, 1435 (2000).
[56] P. Snabre, L. Brunel, and G. Meunier, in *Particle Sizing and Characterization*, edited by T. Provder and J. Texter (American Chemical Society, Michigan, 2004), p. 33.
[57] O. Mengual, G. Meunier, I. Cayre, K. Puech, and P. Snabre, Talanta **50**, 445 (1999).
[58] B. Hoffmann and W. Kohler, J. Magn. Magn. Mater. **262**, 289 (2003).
[59] H. Reerink and J. Th. G. Overbeek, Discuss. Faraday Soc. **18**, 74 (1954).
[60] M. Kerker, *The Scattering of Light and Other Electromagnetic*

Radiation (Academic Press, New York; London, 1969).
[61] R. L. Zollars, J. Colloid Interface Sci. **74**, 163 (1980).
[62] V. G. Vereshchagin, R. A. Dynich, and A. N. Ponyavina, J. Appl. Spectrosc. **65**, 267 (1998).
[63] M. Elimelech, J. Gregory, X. Jia, and R. Williams, *Particle Depostion & Aggregation Measurement, Modelling and Simulation* (Butterworth-Heinemann Ltd, Oxford, 1995).
[64] R. E. Rosensweig, *Ferrohydrodynamics* (Dover, New York, 1997).
[65] P. C. Fannin and S. W. Charles, J. Phys. D **22**, 187 (1989).
[66] J. P. Embs, S. May, C. Wagner, A. V. Kityk, A. Leschhorn, and M. Lücke, Phys. Rev. E **73**, 036302 (2006).